

# Energetics and atomic mechanisms of dislocation nucleation in strained epitaxial layers

O. Trushin<sup>1</sup>

*Institute of Microelectronics and Informatics, Academy of Sciences of Russia, Yaroslavl 150007, Russia*

E. Granato

*Laboratório Associado de Sensores e Materiais,  
Instituto Nacional de Pesquisas Espaciais,  
12201-970 São José dos Campos, SP Brasil*

S.C. Ying

<sup>2</sup>*Department of Physics, Brown University, Providence, RI 02912 USA*

P. Salo and T. Ala-Nissila<sup>2</sup>

<sup>1</sup>*Helsinki Institute of Physics and Laboratory of Physics,  
Helsinki University of Technology, FIN-02015 HUT, Espoo, Finland*

(Dated: July , 2003)

We study numerically the energetics and atomic mechanisms of misfit dislocation nucleation and stress relaxation in a two-dimensional atomistic model of strained epitaxial layers on a substrate with lattice misfit. Relaxation processes from coherent to incoherent states for different transition paths are studied using interatomic potentials of Lennard-Jones type and a systematic saddle point and transition path search method. The method is based on a combination of repulsive potential minimization and the Nudged Elastic Band method. For a final state with a single misfit dislocation, the minimum energy path and the corresponding activation barrier are obtained for different misfits and interatomic potentials. We find that the energy barrier decreases strongly with misfit. In contrast to continuous elastic theory, a strong tensile-compressive asymmetry is observed. This asymmetry can be understood as manifestation of asymmetry between repulsive and attractive branches of pair potential and it is found to depend sensitively on the form of the potential.

PACS numbers: 68.55.Ac, 68.35.Gy, 68.90.+g

## I. INTRODUCTION

Emergence of misfit dislocations in heteroepitaxial systems is a long-standing problem in the field of thin film growth<sup>1,2,3,4,5,6,7,8,9,10,11</sup>. Improving the physical properties of semiconductor heterostructures requires controlling the atomistic processes responsible for generation of defects. Thus, understanding the atomistic mechanisms of defect nucleation is crucially important for further progress in the field of heterostructure growth and structural control of nanostructures. In addition, misfit dislocations represent an important problem in fundamental science. While a lot of information about the nature of dislocations has been obtained within the traditional continuum elastic theory, not near as much is known about the details of the underlying atomistic mechanisms through which dislocation nucleation occurs.

Energy-balance arguments for the competition between strain energy build-up and strain relief due to dislocation nucleation in mismatched epitaxial films lead to the concept of an equilibrium critical thickness. This is defined as the thickness at which the energy of the epitaxial state equals that of a state containing a single misfit dislocation. It has been argued that dislocations should appear in the film when the thickness exceeds this critical value<sup>1,2,3</sup>. The predicted critical value from this consideration, however, both from continuous elastic models<sup>3</sup> and

from models incorporating layer discreteness<sup>10</sup>, is much smaller than the observed experimental value for the breakdown of the epitaxial state. This suggests that the defect-free (coherent) state above the equilibrium critical thickness is metastable<sup>11</sup> and the rate of dislocation generation is controlled by kinetic considerations instead.

The idea of strain relaxation as an activated process is supported by experimental results for the temperature dependence of the critical thickness<sup>11,12,13</sup> and it is the fundamental assumption in kinetic semi-empirical models<sup>14</sup>. Physically, the lowest energy barrier for the nucleation of dislocations should correspond to a transition path that initiates from the free surface (with or without defects). Such processes have been considered in a number of studies using continuum models<sup>15,16,17</sup>. However, it has been pointed out that surface steps and surface roughness that are not considered in the continuum models could play an important role for dislocation nucleation<sup>18,19,20</sup>. Thus, atomistic studies are important for a detailed understanding and determination of the possible mechanisms for defect nucleation in epitaxial films. Although the importance of kinetic factors in real experiments have already been emphasized<sup>11</sup> and also investigated in numerical simulations of atomistic models of the growth process<sup>20</sup>, direct determination of the transition path and corresponding energy barrier for misfit dislocation nucleation from an epitaxial film

has been much less explored, and they often require assumptions on the particular structure of the intermediate configuration<sup>21</sup>.

The actual stress relaxation processes starting from the epitaxial coherent state can occur along many different transition paths. The path with the lowest activation energy barrier at the saddle point corresponds to the true nucleation barrier for the generation of a misfit dislocation. For correct determination of this barrier, it is important to investigate different minimum energy paths (MEPs)<sup>22</sup>, from the metastable coherent state to the incoherent state, without assuming a priori any particular form of the intermediate configurations. We have recently carried out such a task which systematically explore the MEPs in the phase space of the system<sup>23,24</sup> based on a combination of the Repulsive Bias Potential (RBP)<sup>25</sup> and the Nudged Elastic Band (NEB) methods<sup>22</sup>. In the previous work<sup>23</sup>, we considered the case of a relatively large misfit of  $f = \pm 8\%$ . We showed that there is indeed a nonzero energy barrier for defect nucleation. Most importantly, however, we showed that both the mechanisms for the initiation of a misfit dislocation and the activation barrier exhibit a strong *tensile-compressive asymmetry* which is sensitive to the range of the interaction potential. A tensile-compressive asymmetry has also been found previously<sup>20,21</sup> in other contexts.

In this work, we present a detailed systematic study of defect nucleation for the same 2D Lennard-Jones system as in Ref. 23. We consider strains in the range  $f = \pm(4 - 8)\%$ , and intermolecular potentials with different ranges.

## II. MODEL

We consider a 2D model of the epitaxial film and substrate where the atomic layers are confined to a plane as illustrated in Fig. 1. Interactions between atoms in the system were modelled by a generalized Lennard-Jones (LJ) pair potential<sup>26</sup> that is modified to ensure that the potential and its first derivative go to zero at a predetermined cut-off distance  $r_c$ :

$$U(r) = V(r), \quad r \leq r_0;$$

$$U(r) = V(r) \left[ 3 \left( \frac{r_c - r}{r_c - r_0} \right)^2 - 2 \left( \frac{r_c - r}{r_c - r_0} \right)^3 \right], \quad r > r_0, \quad (1)$$

where

$$V(r) = \varepsilon \left[ \frac{m}{n - m} \left( \frac{r_0}{r} \right)^n - \frac{n}{n - m} \left( \frac{r_0}{r} \right)^m \right], \quad (2)$$

$r$  is the interatomic distance,  $\varepsilon$  the dissociation energy and  $r_0$  the equilibrium distance between the atoms. This potential for  $m = 12$  and  $n = 6$  is the same that has been used by Dong *et al.*<sup>20</sup> in a recent simulation study. The

equilibrium interatomic distance  $r_0$  was set to a different value  $r_{ss}$ ,  $r_{ff}$  and  $r_{fs}$  for the substrate, film and film-substrate interaction respectively. The parameter  $r_{ff}$  was varied to give a misfit between lattice parameters as

$$f = (r_{ff} - r_{ss})/r_{ss}. \quad (3)$$

For the film-substrate interaction, we set the equilibrium distance  $r_{fs}$  as the average of the film and substrate lattice constants, *i.e.*  $r_{fs} = (r_{ff} + r_{ss})/2$ . A positive misfit  $f > 0$  corresponds to compressive strain and negative to tensile strain when the film is coherent with the substrate. Calculations were performed with periodic boundary conditions in the direction parallel to the film-substrate interface. For large systems, free boundary conditions gave qualitative similar results. In the calculations, the two bottom layers of the five-layer substrate were held fixed to simulate a semi-infinite substrate while all other layers were free to move. Typically, in our calculations each layer contained 50 or more atoms. The central portion of the initial epitaxial film and substrate are shown in Fig.(1).

In the previous work<sup>23</sup> it was found that some features of dislocation nucleation are sensitive to the detailed form of the atomic potentials used. The results presented here are from systematic calculations for different values of cut-off distances for the 5 – 8 potential ( $m = 8$ ,  $n = 5$ ). The advantage of this potential over the conventional 6 – 12 LJ potential is that it is intrinsically longer ranged. Thus, by imposing different cutoff radius  $r_c$ , one can study the influence of the range of the potential on the nucleation of misfit dislocations. The other difference with respect to the 6 – 12 potential is a softer repulsive core. This will lead to a weaker anharmonicity and less asymmetry between the tensile and compressive strain situations.

## III. METHOD

The standard way of generating transition paths through Molecular Dynamics (MD) simulations<sup>27</sup> does not work well in cases where the probability for rare activated events is small. There are now numerous methods which have been constructed to solve this fundamental problem. The MD technique itself has been augmented by various acceleration<sup>28</sup> and sampling schemes<sup>29,30</sup>. In addition, there is a class of methods that do not evaluate the dynamics directly but instead focus on a systematic search of transition paths and related saddle points for many-particle systems<sup>31,32,33,34</sup>.

We have recently introduced<sup>25</sup> a particularly simple but efficient method called the Repulsive Bias Potential (RBP) method for transition path searching. In the RBP method, the potential energy of the system is augmented with a fixed, repulsive bias potential to make the initial configuration unstable, but to keep the other nearby minima unaffected:

$$U_{\text{tot}}(\vec{r}, \vec{r}_0) = U(\vec{r}) + A \exp\{-[(\vec{r} - \vec{r}_0)/\alpha]^2\}. \quad (4)$$

Here  $U(\vec{r})$  is the original potential energy surface of the system, which has been modified by an exponentially decaying, spherically symmetric potential of strength  $A$  and range  $\alpha$  which is centered at  $\vec{r}_0$ . When  $A$  and  $\alpha$  have been chosen appropriately, forces computed from Eq. (1) can be used to displace the system from its initial state located at  $\vec{r}_0$  to escape to a nearby minimum. This is done by applying total energy minimization to  $U_{\text{tot}}$ .

With the RBP method implemented, the procedure of determining the transition path comprises several stages. First, the initial epitaxial state is prepared by minimizing the total energy of the system using MD cooling. In the MD cooling method, the energy is gradually minimized by setting the velocities  $\mathbf{v} = 0$  whenever  $\mathbf{v}$  and the force  $\mathbf{f}$  on a particle satisfy the condition  $\mathbf{v} \cdot \mathbf{f} < 0$ . Positions and velocities of the particles are obtained from numerical integration of the equations of motion using the standard leap-frog algorithm. Following this, the RBP is applied and the system is slightly displaced from the initial state (randomly or in a selective way to escape from harmonic basin) and then total energy minimization is applied to find a new minimum energy state.

It is important to note that the RBP method can generate many different final states depending on both the initial displacements and the exact form of the repulsive bias introduced. By making the repulsive bias sufficiently localized around the initial potential minimum, the final state energy depends only on the true potential of the system and not on the fictitious repulsive bias. In this work, we only consider the final configurations corresponding to the presence of a single misfit dislocation. Rather than trying random initial displacements, some knowledge of the dislocation generation mechanism is useful for expediting the process.

We also find that the proper choice of initial displacements depends on the sign of the misfit. In the case of compressive strain, to get an ideal single dislocation located in the center of our sample, the optimal initial displacement corresponds to moving one atom in the middle of the first layer of the film from the film-substrate interface upwards by a small distance ( $0.04r_{\text{ss}}$ ). In case of tensile strain, the corresponding optimal initial displacement is a small displacement ( $0.04r_{\text{ss}}$ ) downwards for an atom located in the middle of the second layer in the film from the film-substrate interface layer.

While the repulsive bias potential minimization can be used to generate the final state configuration containing a misfit dislocation, it does not yield the precise minimum energy path and the lowest activation barrier value for getting to this final state configuration. For this purpose, we use the Nudged Elastic Band (NEB) method<sup>22</sup>. This is an efficient method for finding the minimum energy path (MEP), given the knowledge of both initial and final states. The MEP is found by constructing an initial set of configurations (images) of the system between the initial and final states. This set is then allowed to relax to the true set representing the MEP.

An initial guess for the images in the NEB is usually

obtained by interpolating the particle configurations between the final and initial states. For the present application, however, we find that this often leads to numerical instabilities due to the strong hard core repulsion of the LJ potentials and fail to converge to the true MEP. To circumvent this problem, we use the set of configurations generated in moving to the final state in the presence of the repulsive bias as the initial input in the NEB. This leads to fast convergence in the NEB method without the instabilities encountered in the linear interpolation scheme.

## IV. RESULTS

For epitaxial films above the equilibrium critical thickness, the relaxed state with a nonzero density of misfit dislocations which partially relieves the strain energy in the film is expected to have a lower energy. However, if this configuration is separated from the coherent state by a finite energy barrier  $\Delta E$ , the film will remain coherent unless defects are nucleated allowing to overcome this energy barrier. This barrier could be finite even when the relaxed state has already a lower energy than the epitaxial state. Thus the experimentally observed critical thickness can be much larger than the equilibrium value depending on the kinetics of defect nucleation. Our preliminary results<sup>23,24</sup> showed a large variety of relaxation processes, including single dislocation nucleation, multiple dislocations, dislocations with different core structures, and dislocations nucleating on different depth in the film, which can be characterized by their different activation energies and energies of the final incoherent states. In this work, we focus on the nucleation and MEP leading to a final state containing only a single misfit dislocation with core located near the film-substrate interface. To simplify the discussions, we will present in this section only the results for the 5–8 potential with a cutoff radius of  $r_c = 1.5r_{\text{ss}}$ , and lateral size  $L = 50$ , corresponding to 50 atoms per layer. These results allow us to arrive at a simple physical picture for the nucleation process of the misfit dislocation. The results with different parameters for the intermolecular potential and different size of the system are qualitatively similar. They will be presented in a later section.

### A. Mechanisms of relaxation

Relaxation of strain with dislocation nucleation is a complex process involving motion of many particles inside the system. The transition from coherent to dislocated state considered in this paper is analogous to strain relaxation in a real heteroepitaxial sample under annealing conditions. Experiments show that heating is an essential prerequisite for such relaxation to occur<sup>11,13</sup>. This fact shows that nucleation of dislocation represents typical activated process with a nonzero activation barrier.

Our calculations with NEB confirm this conclusion<sup>23,24</sup>. For both the compressive and tensile strain cases, we find the presence of a finite activation barrier  $\Delta E$  along the MEP leading from the initial epitaxial state to the final state with a single misfit dislocation in the film substrate interface. To allow for comparison of different cases and extraction of the basic physics involved, we introduce the definition of the reaction coordinate  $S$ . This is defined as the accumulated displacement of the system along the MEP in the multidimensional configuration space. Mathematically, the reaction path coordinate for a given configuration (image) along the MEP is defined as

$$S_M = \sum_{m=1}^M \sqrt{\sum_{i=1}^N (r_i^m - r_i^{m-1})^2 / N} \quad (5)$$

Here  $M$  is the label for the configuration (image) under consideration, and  $i$  is the index for the different particles in the system ( $i=1$  to  $N$ ). In Fig.(2) and Fig.(3), we show typical snapshots of configurations along the corresponding MEP for compressive and tensile strain cases respectively. In all cases the initial state was an epitaxial film with a coherent interface and the final state contained a single dislocation with its core located in the interface layer. The final state is characterized by the presence of an adatom island on the surface of the film in the case of compressive strain and a vacancy island in the tensile case. The number of adatoms (or vacancies) in the island exactly corresponds to the number of layers in the film. Such form of the final state is determined by the geometry of the misfit dislocation, as the one extra atom is added or removed from (or inside) each layer to relax the strain.

An important property of the NEB method is that it usually converges to the MEP nearest to the initial trial trajectory. Thus by changing the initial input path, we were able to investigate several different mechanisms of relaxation<sup>23,24</sup>. These mechanisms differ from each other mainly by the level of collectiveness in the displacement of the particles from the coherent state position. For each given set of parameters, we identify the lowest activation barrier. The particular kind of mechanism leading to the lowest activation barrier depends on the parameters of model (misfit, cut-off radius of potential *etc.*). We find that for all the systems that we have studied, the mechanisms leading to the lowest activation barrier belong to one of the two categories described below.

The first mechanism describing the transition from the initial coherent state to the final state with a misfit dislocation at the film substrate interface corresponds to a successive sliding along the edges of a triangle. The saddle point configurations corresponding to this mechanism for the tensile and compressive strain cases are shown in Fig. (4a) and Fig. (4b) respectively. We see that in this case the displacements of the atoms have a collective behavior, with two edges of a triangle successively sliding up or down (one by one). Eventually, an adatom island

or a vacancy island is created on the surface of the film. The highest saddle point can correspond either to the sliding of the first or the second edge. We refer to this as the glide mechanism since the motion of the dislocation after it is nucleated follows the path referred in the literature as dislocation glide<sup>4</sup>. For the tensile strained film, the glide mechanism always yield the lowest activation barrier. While for the compressively strained film, the mechanism leading to the the lowest activation barrier depends actually on the magnitude of the misfit. For small misfit ( $f \leq 8\%$ ), the glide mechanism is again the one leading to the lowest activation barrier. This is drastically different from the climb mechanism reported earlier<sup>23</sup> for a misfit of 8% in a compressively strained film.

The second mechanism correspond to successive relaxation of layers. This is the preferred mechanism for a compressively strained film with large misfits ( $f \geq 8\%$ ). The saddle point configuration corresponding to this mechanism for the compressive strain of 8% misfit is shown in Fig.(4c). In this case, the core of the dislocation first appears at either the second or the third layer of the film and then successively moves down from layer to layer to the film-substrate interface. The displacement of the particles have a very localized character in this kind of mechanism. We refer to this as the climb mechanism since the motion of the dislocation after it is first nucleated in this case corresponds to what is known in the literature as dislocation climb<sup>4</sup>. For intermediate values of compressive strain, the situation is more complicated, as the two mechanisms are competitive in energy costs. The actual MEP in this case is better described by a mixture of the climb and glide mechanisms.

## B. Activation energy of dislocation nucleation

The most important characteristic of a particular relaxation process through nucleation of a misfit dislocation is its activation energy  $\Delta E$ . The activation barrier is calculated as the difference between the total energy of the initial state and that of the saddle point configuration. As can be seen in Fig. (2), corresponding to the compressive strain case, there may exist many saddle points along a given MEP. The activation barrier is determined by the highest energy saddle point. The results for  $\Delta E$  vs. the number of layers in the film are presented in Fig.(5).

For the tensile strain case, we find that the process leading to the nucleation of misfit dislocation and subsequent motion along the MEP is always through the glide mechanism. The activation barrier decreases with increasing magnitude of misfit. Also, at large misfits, the activation barrier decreases significantly as the film thickness increases, leading to an essentially negligible activation barrier. This was verified directly through independent MD simulation at finite temperatures where the misfit dislocation is easily generated spontaneously.

For the compressive strain case, except at 4% misfit and small thickness (less than six layers), the barriers are higher than the corresponding tensile strain case with the same magnitude of misfit. Again, there is a strong decrease in  $\Delta E$  with increasing magnitude of misfit. In contrast to the tensile strain case, the activation barrier tends to level off with increasing film thickness. The other striking difference from the tensile strain case is that the mechanism corresponding to the movement along the MEP in this case can either be the glide mechanism as in the tensile strain case, or the qualitatively totally different climb mechanism involving layer by layer distortion as discussed in the last section. This new climb mechanism occurs for large misfits ( $f \geq 8\%$ ).

## V. SIMPLE PHYSICAL PICTURE FOR THE NUCLEATION PROCESS

As shown in the last section, the mechanism leading to the nucleation of a misfit dislocation starting from the epitaxial coherent state and the subsequent motion along the MEP to the final state is fairly complicated, and depends sensitively on the sign and magnitude of the misfit (tensile or compressive strain), and thickness of the film. With this rich set of data, it is important to have some simple qualitative understanding of the results.

First of all, it is easy to understand the origin of the difference between the tensile and compressive strain cases. In a harmonic elasticity theory, the activation barrier would depend only on the magnitude and not the sign of the strain. The tensile-compressive asymmetry thus originates from the strong anharmonicity of the interaction potential, particularly in the steeply rising repulsive core. This is confirmed by our results shown in Fig.(5) showing that the difference of  $\Delta E$  for the tensile and compressive cases grows monotonically as the misfit increases in magnitude. This is also confirmed in our similar studies using the conventional 6 – 12 LJ potential as shown in Fig.(6). Since the 6 – 12 potential is considerably steeper in the core region, the anharmonicity is stronger and the resulting tensile-compressive asymmetry is even more pronounced.

The other general trend is the strong decrease of the activation barrier with increasing misfit. This is true for both the tensile and compressive cases (Fig. 5). It remains true even when the mechanism leading to the nucleation has changed character from a glide nature to a climb nature as in the case of large compressive strain. In our previous work<sup>23</sup>, we have analyzed the contribution to the activation barrier from the intralayer and interlayer bond distributions at the saddle point. Here we will introduce the same physical arguments in terms of the conceptually simpler quantity of reaction coordinate defined earlier in Eq. (5). Let  $S$  represent the dimensionless reaction coordinate along the MEP leading from the initial coherent state through the saddle point to the final state containing the misfit dislocation. For the initial

stages of small displacement with  $S \ll 1$ , the simplest leading representation of the MEP can be expressed in the form

$$E = \frac{a}{2}S^2 - \frac{b}{3}S^3. \quad (6)$$

In the equation above, the first term gives the energy rise towards the saddle point from the initial displacements from the coherent state necessary to nucleate the dislocation. It originates mainly from the stressing of the interlayer bonds which are fully relaxed in the initial coherent epitaxial state. Because of this initial relaxation, there is relatively little dependence of the coefficient  $a$  on the misfit. The second term represents the release of the intralayer strain energy from the displacements of the atoms. Clearly, the coefficient  $b$  is strongly dependent on the magnitude of the misfit. Whether it is tensile or compressive, the higher the magnitude of the strain, the larger is the lowering of the strain energy. Hence the coefficient  $b$  should be a monotonically increasing function of the magnitude of the misfit. It follows simply from Eq. (6) that the activation barrier  $\Delta E$  is given by the expression

$$\Delta E = \frac{1}{6} \frac{a^3}{b^2}. \quad (7)$$

Thus, the activation barrier always decreases with increasing magnitude of the strain, whatever the actual initial strain release mechanism and nature of the saddle point configuration. Furthermore, the expression in Eq. (6) predicts that the saddle point should occur at the reaction coordinate  $S_0 = a/b$  which again decreases monotonically as the misfit magnitude increases. This is supported by our results as shown in Fig.(7).

In general, the initial cost of energy in creating the distortion for the dislocation in the glide mechanism is lower for a tensile than compressive strain. This is due to the fact that for the compressive strained film, the initial distortion required for creating the dislocation core always involve breaking of bonds to lower the coordination number. On the other hand, for the tensile strained film, no breaking of bonds is necessary in the glide mechanism for the nucleation of the dislocation. Thus the glide mechanism is always preferred for the tensile strained film. For the large compressive strain, the energy cost involved in nucleating a dislocation core is comparable for the glide and climb mechanism, and the two processes are competitive.

The dependence of the activation barrier on the film thickness is more complicated and is rather different for the tensile and compressive strains. For the large compressive strain case where the MEP corresponds to the climb mechanism, the behavior is fairly easy to understand as the saddle point involves a rather localized dislocation in the surface layers, so obviously the activation barrier would have a very weak dependence on the film thickness as observed in our numerical study. For the glide mechanism, both the initial rise in energy and the

release of the strain energy leading to the saddle point configuration are dependent on the film thickness and according to Eq. (6), it is hard to predict any universal dependence of the activation barrier on the film thickness. Indeed, both a levelling off (for compressive strain) and a strong decrease in the activation barrier as a function of the film thickness have been observed.

## VI. SIZE AND POTENTIAL DEPENDENCE

The results presented in the previous sections are all for a 5 – 8 short ranged L-J potential with a cutoff set at  $1.5r_{ss}$ . The size of the system was set at  $L = 50$  particles per layer. We have also performed similar calculations for different set of parameters in the potential as well as for different sizes to investigate the size and potential dependence of our results. We find that the results with different interatomic potentials and sizes of the system are qualitatively similar, although differing in details. We present some of these results in this section.

In Fig. (8), the activation energy barrier is plotted against the film thickness for a system size of  $L = 20$  and a short ranged potential as in the previous sections for two values of the magnitudes of misfit at  $|f| = 5\%$  and  $8\%$ . The results are very similar to that presented in Fig. (5). The only limitation for the smaller sample size is that one cannot accurately study the cases of smaller misfit as the addition or removal of a single atom from a layer would overshoot the strain release mechanism.

In Fig. (9), we show the results of activation energy barrier vs film thickness for system size  $L = 50$  and a 5 – 8 LJ potential as before but this time with a longer range with cutoff set at  $2.1r_{ss}$ . Again, the results are qualitatively similar to that presented in Fig. (5). The tensile and compressive asymmetry is stronger for this longer ranged potential, particularly at the smaller misfit values. This could be also related to the stronger size

effects for the longer ranged potential.

## VII. CONCLUSIONS

We have developed a general scheme of identifying minimal energy paths for spontaneous generation of misfit dislocation in an epitaxial film and studied the energetics and atomic mechanisms of stress relaxation using a two-dimensional model. This approach requires no a priori assumptions about the nature of the transition path or the final states. A nonzero activation barrier for dislocation nucleation is found in the minimum energy path from coherent to incoherent state. We find that the energy barrier decreases strongly with misfit. The nucleation mechanism from a flat surface depends crucially on whether we start from a tensile or compressive initial state of the film. This asymmetry originates from the anharmonicity of the interaction potentials which leads to qualitatively different transition paths for the two types of strains. The present method can also be extended to three-dimensional models with more realistic interaction potentials. Preliminary calculations for a three-dimensional Lennard-Jones system and the Pd/Cu and Cu/Pd systems<sup>35</sup> with the Embedded Atom Model potentials<sup>36</sup> confirms the effectiveness of the method in three dimensions.

## VIII. ACKNOWLEDGEMENTS

This work has been supported in part by Fundação de Amparo à Pesquisa do Estado de São Paulo - FAPESP (grant no. 03/00541-0) (E.G.), the Academy of Finland through its Center of Excellence program (T.AL and P.S.) and by a NSF-CNPq grant (E.G. and S.C.Y.).

<sup>1</sup> J.C. Bean, Science **230**, 127 (1985).

<sup>2</sup> J. W. Matthews and A. E. Blakeslee, J. Cryst. Growth **27**, 118 (1974).

<sup>3</sup> C. A. B. Ball and J. H. van der Merwe, in *Dislocation in Solids*, F. R. N. Nabarro, Ed. (North-Holland, Amsterdam, 1983).

<sup>4</sup> P. Politi, G. Grenet, A. Marty, A. Ponchet, and J. Villain, Physics Reports **324**, 271(2000).

<sup>5</sup> C.M. Gilmore and V. Provenzano, Phys. Rev. B **42**, 6899 (1990).

<sup>6</sup> B.W. Dodson and P.A. Taylor, Appl. Phys. Lett. **49**, 643 (1986).

<sup>7</sup> P. A. Taylor and B.W. Dodson, Phys. Rev. B **36**, 1355 (1987).

<sup>8</sup> A.S. Nandedkar, G.R. Srinivasan, and C.S. Murthy, Phys. Rev. B **43**, 7308 (1991).

<sup>9</sup> F. Much, M. Ahr, M. Biehl, and W. Kinzel, Europhys. Lett. **56**, 791 (2001).

<sup>10</sup> E. Granato, J.M. Kosterlitz, and S.C. Ying, Phys. Rev. B **39**, 3185 (1989).

<sup>11</sup> J. Y. Tsao, B. W. Dodson, S. T. Picraux, and D. M. Cornelison, Phys. Rev. Lett. **59**, 2455 (1987).

<sup>12</sup> H. Luth in *"Surfaces and Interfaces of Solid Materials"*, Springer 1998.

<sup>13</sup> J. Zou and D. J. H. Cockayne, and B. F. Usher, Appl. Phys. Lett. **68**, 673 (1996).

<sup>14</sup> D. C. Houghton, J. Appl. Phys. **70**, 2136 (1991).

<sup>15</sup> B. J. Spencer, P. W. Voorhees, and S. H. Davis, Phys. Rev. Lett. **67**, 3696 (1991).

<sup>16</sup> A. G. Cullis, A. J. Pidduck, and M. T. Emeny, Phys. Rev. Lett. **75**, 2368 (1995).

<sup>17</sup> J. Grilhé, Europhys. Lett. **23**, 141 (1993).

<sup>18</sup> S. Brochard, P. Beauchamp, and J. Grilhé, Phil. Mag. A **80**, 503 (2000).

<sup>19</sup> J. Tersoff and F. K. LeGoues, Phys. Rev. Lett. **72**, 3570 (1994).

- <sup>20</sup> L. Dong, J. Schnitker, R. W. Smith, and D. J. Srolovitz, *J. Appl. Phys.* **83**, 217 (1998).
- <sup>21</sup> M. Ichimura and J. Narayan, *Phil. Mag. A* **72**, 281 (1995).
- <sup>22</sup> H. Jónsson, G. Mills and K. W. Jacobsen, in *Classical and Quantum Dynamics in Condensed Phase Simulations*, ed. by B. J. Berne *et al* (World Scientific, Singapore, 1998).
- <sup>23</sup> O. Trushin, E. Granato, S.-C. Ying, P. Salo and T. Ala-Nissila, *Phys. Rev. B*, **65**, 241408, (2002).
- <sup>24</sup> O. Trushin, E. Granato, S.-C. Ying, P. Salo and T. Ala-Nissila, *Phys. Stat. Sol. B*, **232**,100,(2002).
- <sup>25</sup> O. Trushin, P. Salo, T. Ala-Nissila, and Ying, unpublished.
- <sup>26</sup> S. Zhen and G. J. Davies, *Phys. Stat. Sol. A* **78**, 595 (1983).
- <sup>27</sup> T. Rasmussen, *Phys. Rev. B* **62**, 12664 (2000).
- <sup>28</sup> A. F. Voter, F. Montalenti, and T. C. Germann, *Annu. Rev. Mater. Res.* **32**, 321 (2002).
- <sup>29</sup> C. Dellago, P. G. Bolhuis, F. S. Csajka, and D. Chandler, *J. Chem. Phys.* **108**, 1964 (1998); C. Dellago, P. G. Bolhuis, and D. Chandler, *J. Chem. Phys.* **108**, 9236 (1998).
- <sup>30</sup> L. Y. Chen and S. C. Ying, *Phys. Rev. B* **60**, 16965 (1999); L. Y. Chen, S. C. Ying, and T. Ala-Nissila *Phys. Rev. E* **65**, 042101 (2002).
- <sup>31</sup> G. T. Barkema and N. Mousseau, *Phys. Rev. Lett.* **77**, 4358 (1996).
- <sup>32</sup> L. J. Munro and D. J. Wales, *Phys. Rev. B* **59**, 3969 (1999).
- <sup>33</sup> G. Henkelman and H. Jónsson, *J. Chem. Phys.* **111**, 7010 (1999).
- <sup>34</sup> N. Mousseau and G. T. Barkema, *Phys. Rev. B* **61**, 1898 (2000).
- <sup>35</sup> O. Trushin *et al*, unpublished.
- <sup>36</sup> S. M. Foiles, M. I. Baskes, and M. S. Daw, *Phys. Rev. B* **33**, 7983 (1986).

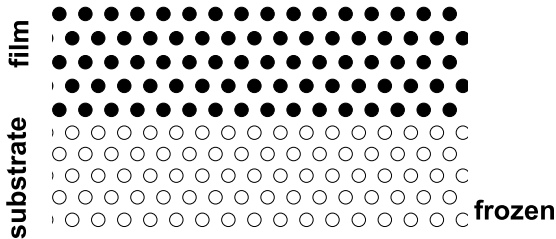


FIG. 1: A 2D model of the epitaxial film and substrate showing the particle configurations in the coherent state. The two layers at bottom are held fixed while all other are free to move. Filled circles represent the the epitaxial film and open circles the substrate.

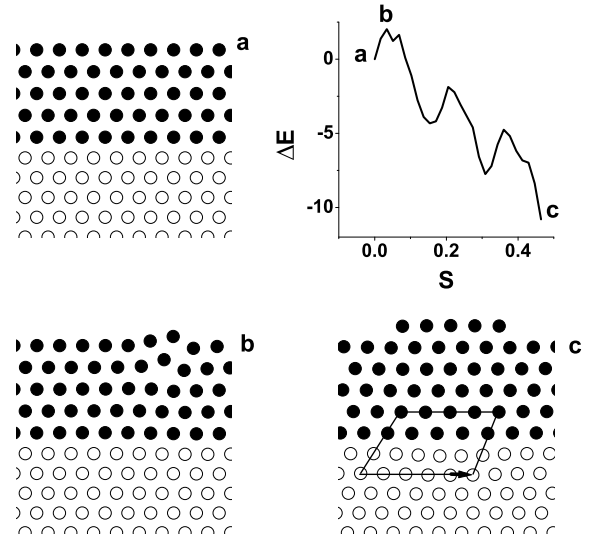


FIG. 2: Minimal Energy path for compressive strain  $f = +8\%$  as a plot of energy barrier  $\Delta E$  vs reaction coordinate  $S$ . Snapshots configurations (a), (b) and (c) correspond to the labels in the energy profile (top right). Closed line in (c) is the Burgers circuit around the dislocation core. The energy barrier is in units of interatomic potential strength  $\epsilon$  and the reaction coordinate  $S$  is in units of equilibrium distance  $r_{ss}$ .

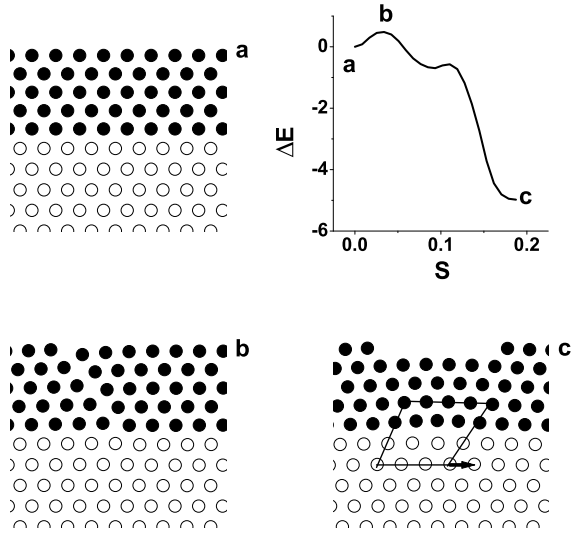


FIG. 3: Minimum Energy path for tensile strain  $f = -8\%$  as a plot of energy barrier  $\Delta E$  vs reaction coordinate  $S$ . Snapshots configurations (a), (b) and (c) correspond to the labels in the energy profile (top right). Closed line in (c) is the Burgers circuit around the dislocation core. The energy barrier is in units of interatomic strength  $\epsilon$  and the reaction coordinate  $S$  in units of equilibrium distance  $r_{ss}$ .

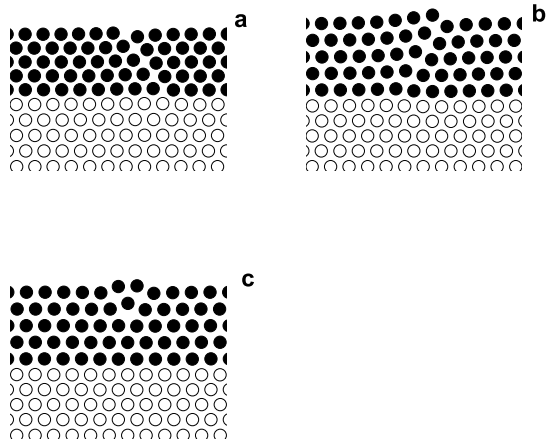


FIG. 4: Saddle point configurations for different mechanisms of stress relaxation (a) glide mechanism for tensile strain (b) glide mechanism for compressive strain (c) climb mechanism for compressive strain. Filled circles represent the the epitaxial film and open circles the substrate.

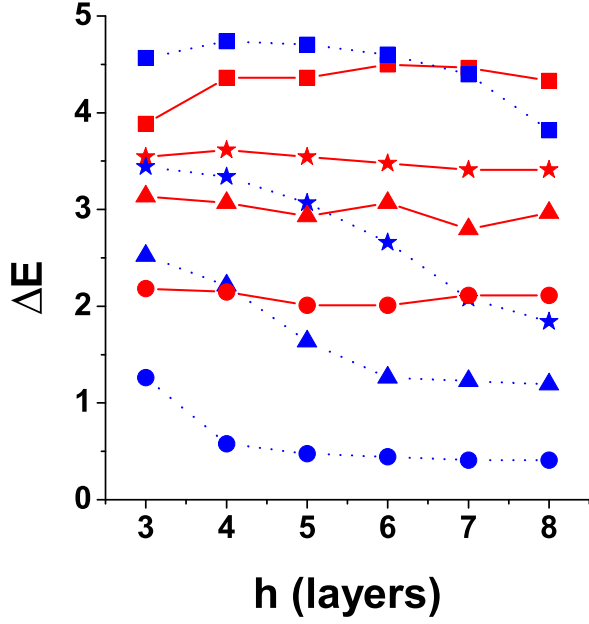


FIG. 5: Energy barrier  $\Delta E$  (in units of  $\epsilon$ ) as a function of film thickness (number of layers) for different misfit values. Squares symbols correspond to  $f = \pm 4\%$ , stars to  $f = \pm 5\%$ , triangles to  $f = \pm 6\%$ , and circles to  $f = \pm 8\%$ . Solid and dotted lines correspond to compressive  $f > 0$  and tensile  $f < 0$  strains, respectively.

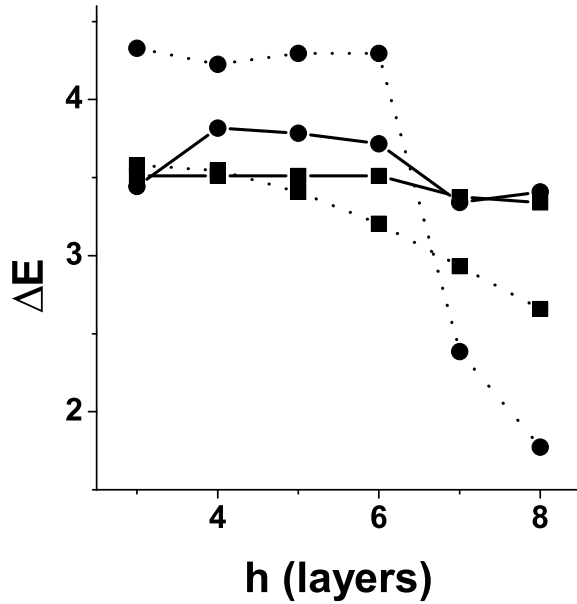


FIG. 6: Energy barrier  $\Delta E$  (in units of  $\epsilon$ ) as a function of film thickness (number of layers) at misfit 5%, for the 5 – 8 (squares) potential and 6 – 12 (circles) potential (cut off  $1.5r_{ss}$ ). Solid and dotted lines correspond to compressive  $f > 0$  and tensile  $f < 0$  strains, respectively. Here the system size is  $L = 20$ .

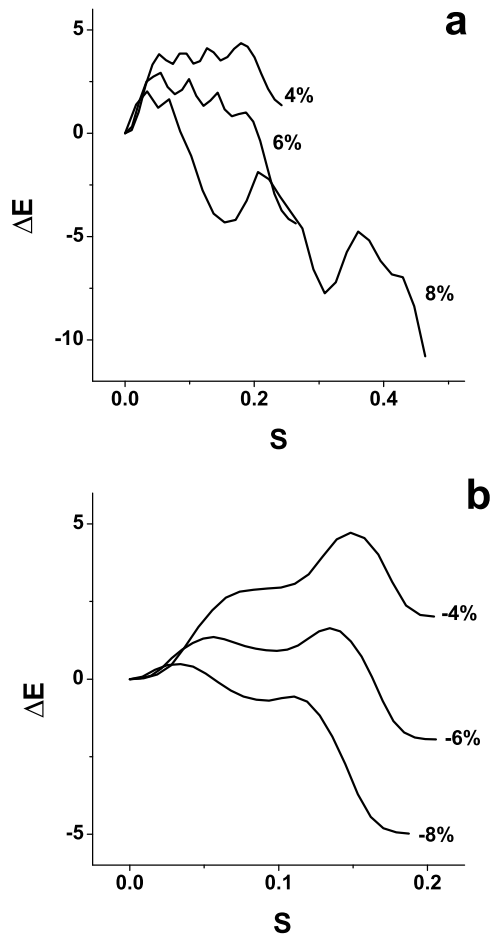


FIG. 7: Energy profile of the minimum energy path for (a) compressive and (b) tensile strain and for different misfits. Energy in units of  $\epsilon$  and  $S$  in units of equilibrium distance  $r_{ss}$ .

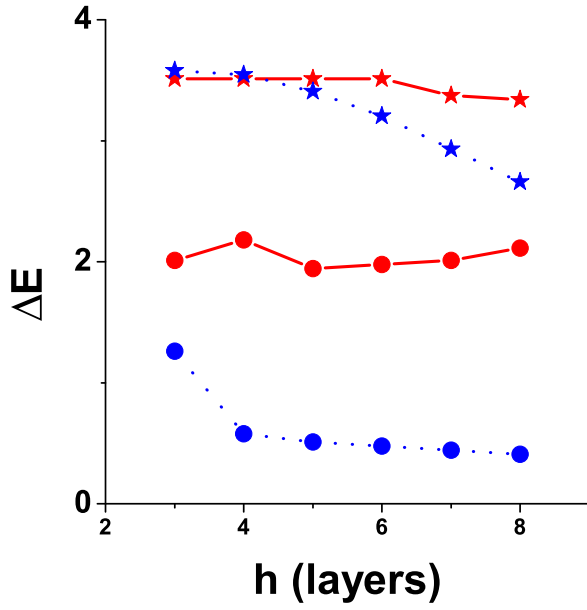


FIG. 8: Energy barrier  $\Delta E$  (in units of  $\epsilon$ ) as a function of film thickness (number of layers) for smaller sample size (20 atoms per layer) and different misfit values for the 5–8 potential:  $f = \pm 5\%$  (stars), and  $f = \pm 8\%$  (circles). Solid and dotted lines correspond to compressive  $f > 0$  and tensile  $f < 0$  strains, respectively.

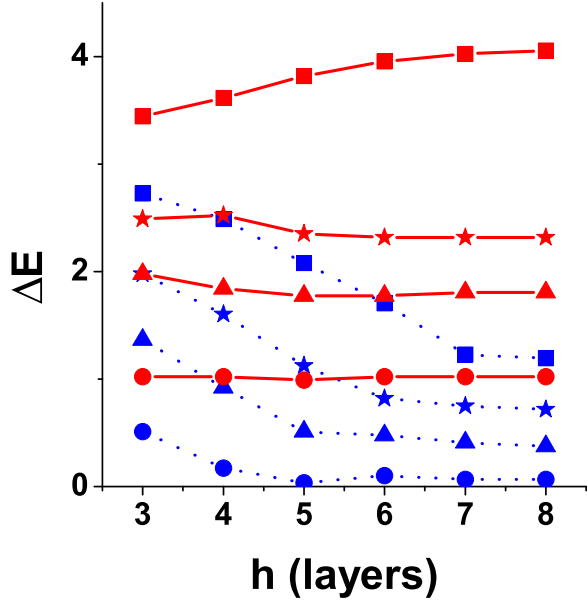


FIG. 9: Energy barrier  $\Delta E$  (in units of  $\epsilon$ ) as a function of film thickness (number of layers) for different misfit values for long ranged 5–8 potential (cut off  $2.1r_{ss}$ ):  $f = \pm 4\%$  (squares),  $f = \pm 5\%$  (stars),  $f = \pm 6\%$  (triangles), and  $f = \pm 8\%$  (circles). Solid and dotted lines correspond to compressive  $f > 0$  and tensile  $f < 0$  strains, respectively.